DOI: 10.1002/anie.201107824

Biomineralization

Controlling Nanostructures of Mesoporous Silica Fibers by Supramolecular Assembly of Genetically Modifiable Bacteriophages**

Chuanbin Mao, Fuke Wang, and Binrui Cao*

Well-ordered mesoporous silica has been successfully prepared using cationic quaternary ammonium surfactants (M41S family),[1] nonionic surfactants (SBA family),[2] and anionic surfactants.[3] As a result of their attractive properties, that is, large surface areas and uniform pore sizes, numerous versatile applications of mesoporous silica have been reported in catalysis, bioabsorption, drug delivery, and nanoreactors.[4] It is generally accepted that the formation of well-ordered mesoporous silica involves both charge matching and cooperative assembly of surfactant micelles and silicate into 3D lattice structures such as hexagonal, cubic, or lamellar.[5]

Biological particles are also good templates for the formation of silica.[6] Moreover, nature has designed filamentous viruses such as *M13* and *fd* bacteriophage that are morphologically similar to rodlike micelles yet possess a greater monodispersity than surfactant micelles. In addition, they readily form a lyotropic liquid-crystalline (LC) phase through self-assembly. As an example, the semiflexible rodlike bacteriophages (*fd* or *M13*) used in this study are bacteria-specific viruses (about 880 nm long and about 7 nm wide) that can be pictured as an ordered assembly of coat proteins along circular ssDNA (see Figure S1 in the Supporting Information). They have high aspect ratios and are capable of self-assembling into LC structures.[7] Such a high degree of monodispersity and anisotropy of bacteriophage, however, has never been successfully employed in synthesizing mesoporous silica with ordered pore lattices.

Here, we report the preparation of well-ordered mesoporous silica fibers with hexagonally arranged pores (termed OU-880) by use of filamentous bacteriophages as templates. In addition, we discuss the successful use of the resultant mesoporous silica as a means for fabricating 3D arrays of PbS nanoparticles. Nature creates incredibly sophisticated mineral structures through the self-assembly of specific proteins that direct biomineralization at ambient conditions.[8] As one of the most prominent examples, diatoms form fine micro-/nanostructured silica walls under the direction of assembled siliffins.[9] Therefore, we also explore the ability of bacteriophages to control the nanostructures of silica by controlling their self-assembly behavior.

Since foreign peptides can be genetically fused to the coat proteins of bacteriophage to produce highly decorated viruses,[10] and the assembly behavior of bacteriophage is strongly affected by its surface charge properties, bacteriophage presents itself as an excellent candidate template for controlling resulting silica nanostructures.[11] By displaying peptides with different charges on the side wall of filamentous bacteriophage, we demonstrate the successful controlling of silica nanostructures through control of the bacteriophage surface charge density and the concomitant bacteriophage assembly behavior.

Both wild-type and genetically engineered bacteriophage were used as templates for fabricating silica. Wild-type bacteriophage *fd* is a polyelectrolyte with a molecular weight (MW) of $1.67\times10^7\,g\,mol^{-1}$, and a charge density of 10*e* per nanometer in water at pH 8.1.[12] *M13* bacteriophage is almost identical to *fd* with the exception that the 12th negatively charged residue (Asp) of each major coat protein (pVIII, Figure S1) in *fd* is replaced by a polar one (Asn) in *M13*.[13] Each virus consists of a ssDNA molecule packed in a sheath of about 3000 identical coat proteins. As a result, *M13* has an approximately one quarter reduction in the surface charge density. Four minor coat proteins (pIII, pVI, pVII, and pIX) additionally cap the two ends of the filamentous phage (see Figure S1 in the Supporting Information).[14] A foreign peptide can be genetically fused to the N-terminal of pVIII, enabling genetic controlling of the side wall surface chemistry of bacteriophage.[15]

The preparation of mesoporous silica was achieved by employing 3-aminopropyltriethoxysilane (APTES) as a co-structure-directing agent and prehydrolyzed tetraethoxysilane (TEOS), which was prepared by stirring TEOS in deionized (DI) water overnight, as a growth agent. In a typical experiment, APTES was first added to an *fd* virus suspension ($20\,mg\,mL^{-1}$) in DI water. The resulting mixture was incubated at room temperature for about 3 min followed by the addition of excessive prehydrolyzed TEOS. Vortexing was applied for about 3–5 min after addition of TEOS to the virus suspension to ensure a good dispersion of TEOS within the mixture. Although white flocculates appeared within 15 min, the reaction mixture was allowed to stand at room temperature for 8 h. OU-880 was then collected by centrifugation and washed with ethanol and water several times before being dried at 70 °C. Some samples were further calcined at 550 °C

[*] Prof. C. B. Mao, F. Wang, B. Cao
Department of Chemistry and Biochemistry
Stephenson Life Sciences Research Center, University of Oklahoma
101 Stephenson Parkway, Norman, OK 73019-5251 (USA)
E-mail: cbmao@ou.edu

[**] We thank the National Science Foundation (grant numbers DMR-0847758, CBET-0854414, and CBET-0854465), the National Institutes of Health (grant numbers 5R01HL092526-02, 5R21EB009909-02, and 4R03AR056848-03), the Department of Defense Congressionally Directed Medical Research Program, the Oklahoma Center for Adult Stem Cell Research Center, and the Oklahoma Center for the Advancement of Science and Technology (grant number HR11-006) for financial support. We also thank Drs. B. Grady, A. Madden, W. T. Yip, H. Lu, and P. Larson for their kind help during the study.

Supporting information for this article is available on the WWW under http://dx.doi.org/10.1002/anie.201107824.

for 4 h for characterization and applications in templating the growth of nanoparticles.

Both SEM and TEM images showed the formation of silica fibers with a length ranging from several micrometers to tens of micrometers (Figure 1). High-resolution SEM images (Figure 1 a, inset) revealed that these fibers were indeed bundles of narrower silica fibers with uniform diameters ranging from 70–80 nm. High-resolution TEM images of as-synthesized small silica fibers showed uniform and parallel aligned lattice fringes (Figure 1 b), indicating a LC array of bacteriophages in the resulting OU-880.

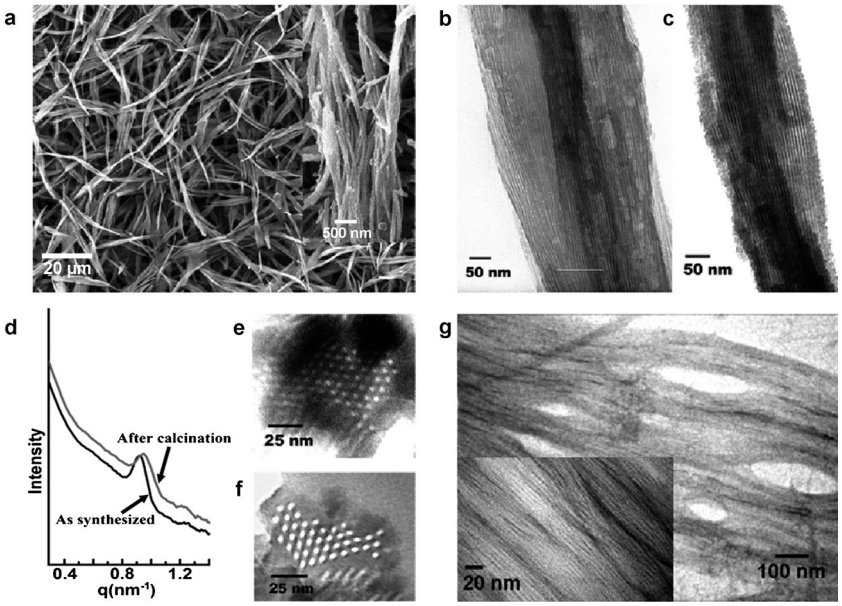

Figure 1. Characterization of bacteriophage-governed mesoporous silica fibers (OU-880). a) SEM images of OU-880 with a range of lengths from several to ten micrometers. The inset shows the high-resolution SEM image of OU-880, indicating that the large fibers were indeed bundles of small uniform nanofibers with diameter of 70–80 nm. b and c) High-resolution TEM images of as-synthesized (b) and calcined (c) OU-880. d) SAXS pattern of the as-synthesized and calcined mesoporous silica fibers (OU-880). e and f) Cross-sectional TEM images of the as-synthesized (e) and calcined (f) OU-880. g) TEM images of the formed bacteriophage bundles induced by APTES interactions. The inset shows the corresponding high magnification TEM image.

Removal of bacteriophages by calcination at 550 °C for 4 h in air gave parallel aligned and uniform sized channels in OU-880 which ran through the entire silica fiber (Figure 1 c). To gain insight into the bacteriophage alignment pattern and lattice spacing within OU-880, the silica fibers were cut by a microtome to form thin cross-sections which were viewed by TEM. As shown in Figure 1 e and 1 f for the cross-sectional TEM images of the as-synthesized and calcined OU-880, respectively, hexagonal arrays of bacteriophages or channels in the obtained silica fibers were observed. The calculated average lattice spacing (channel center-to-center distance) for the as-synthesized and calcined OU-880 was determined as 7.8 and 7.6 nm, respectively. Since the thickness of the silica side wall (between two neighboring bacteriophages) was found to be (2 ± 0.5) nm, the diameter of bacteriophages calculated from lattice spacing (about 5.8 ± 0.5 nm) was slightly less than that of native *fd* bacteriophage (6.6 nm),[12] which was possibly due to compression of biomolecules during silicification.[16]

Hexagonal lattices of the bacteriophage templated OU-880 were then investigated by small angle X-ray scattering (SAXS). The SAXS patterns of both the as-synthesized and calcined OU-880 showed a Bragg peak of low index planes that is typical for a hexagonal lattice, suggesting a long-range order of bulky materials (Figure 1 d). The center-to-center pore spacing was calculated to be 7.8 and 7.6 nm for as-synthesized and calcined OU-880, respectively, which match the result from TEM observation. The decrease of *d* spacing in the calcined OU-880 was due to further condensation of silica during the calcinations. The surface area of OU-880 obtained by the BET method is 341.57 $m^2 g^{-1}$ which is close to the reported results of silica nanotubes (328 $m^2 g^{-1}$ [17] or 332 ± 21 $m^2 g^{-1}$ [18]) with a structure similar to OU-880. The pore diameter calculated (4.871 nm) from the Barrett–Joyner–Halenda (BJH) method matches the pore (channel) diameter measured by TEM (about 5.5 nm; see Figure S2 and the Supporting Information for details).

The hexagonal pore structures of the resulting silica arose from synergistic interactions between bacteriophages, APTES (functioning as co-structure-directing agent) and silicic acid (from prehydrolyzed TEOS).[19] In our experiment, we noted that addition of APTES to the *fd* virus suspension induced the aggregation of viruses, forming a bundle structure (Figure 1 g). APTES binds to individual *fd* bacteriophages by electrostatic interactions and hydrogen bonding between its amino group and surface proteins of virus (see the Supporting Information). Nucleophilic residues at the N-terminal of pVIII such as Lys 8 and Ser 13 may catalyze and initiate the hydrolysis of APTES, forming oligomers or even nanoparticles.[5b,20]

Because of the propyl amine arm in APTES, the formed oligomeric silicic acids contained both positively charged amino groups and negatively charged polysilicic acid (see Figure S3 in the Supporting Information). The formed APTES intermediates functioned as multidentate counterions, attracting neighboring viruses together to form an ordered assembly through electrostatic and hydrogen-bonding interactions (Figure 2 and Figures S1 and S3 in the Supporting Information). The APTES-induced virus assembly was also confirmed by dynamitic light scattering (DLS) and zeta potential (ξ) analysis. DLS results showed the kinetic formation of larger aggregates once APTES was added to the bacteriophage solution (Figure S4 in the Supporting Information). Zeta potential analysis of bacteriophage before and after the addition of APTES showed a remarkable decrease

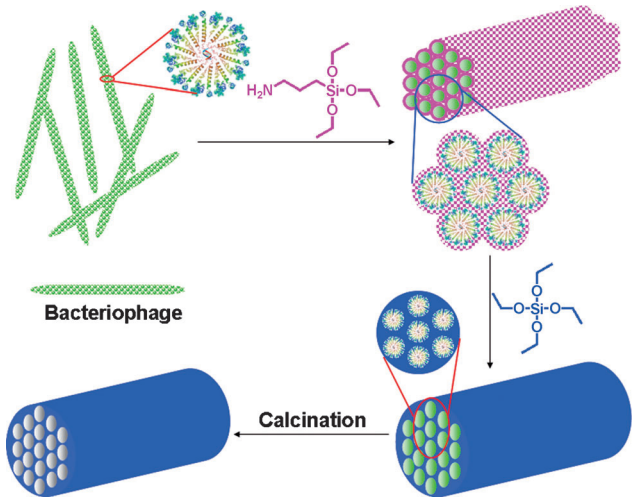

Figure 2. Proposed mechanism for the bacteriophage-directed formation of hexagonal mesoporous silica. The insets show the cross-section view of bacteriophage assemblies. The magenta spots stand for mono- and oligo-hydrolysized APTES molecules which are anchored to the bacteriophage surface and function as nuclei for subsequent polycondensation of TEOS. The blue color illustrates the formed silica network through polycondensation of TEOS on the nuclei.

of mobility and effective surface charge (Figure S5) which was attributed to the virus assembly and phase segregation as observed in the nanofabrication of silica in diatom biosilica.[21]

When prehydrolyzed TEOS was added to the mixture of APTES and bacteriophage, the formed APTES intermediates (oligomeric silicic acids) functioned as seeds initiating the polycondensation of TEOS on the surface of the bacteriophages (Figure 2). As the polycondensation of TEOS proceeded, the charge density of the inorganic layer changed with increase in the thickness of the silica wall. The matching of charge density between the bacteriophage surface and silica species may finally govern the 3D assembly with the lowest interface energy.[5a,22] Furthermore, contributions to the hexagonal organization of bacteriophages in the resulting mesoporous silica include the condensation of bacteriophage from solution through APTES interactions, the semiflexible rodlike structure of bacteriophage, the high degree of monodispersity and the anisotropic polarity of bacteriophages (Figure 2).

Due to the uniform cylindrical pores and unidirectional array of the pores, mesoporous silica has been successfully exploited as templates for the preparation of metal and semiconductor nanowires.[23] However, a unidirectional ordered array of nanoparticles in mesoporous silica has never been successfully attempted. Here, we show the preparation of an ordered 3D array of nanoparticles with preferred nanocrystal orientation along the fiber by taking advantage of the hexagonal arrangement of uniform pores within OU-880.

To prepare a 3D PbS nanoparticle array, OU-880 was first calcined at 550 °C for 4 h to remove any organic composition, followed by immersion in an aqueous solution of saturated lead acetate (PbAc). The OU-880 absorbed with Pb^{2+} was filtered and washed with DI water twice and placed into a chamber filled with H_2S gas. TEM imaging (see Figure S6a in the Supporting Information) confirms that an ordered 3D array of PbS nanocrystals was formed within the channels of OU-880. The uniform diameter of PbS nanoparticles was determined to be (5.5 ± 0.2) nm, which is consistent with the diameter of an individual channel (about 5.5 nm). Corresponding selected area electron diffraction (SAED) analysis indicated that the PbS nanoparticles in the individual channels were oriented with a [100] axis preferentially parallel to the channel (Figure S6b). Energy-dispersive spectroscopy (EDS) analysis (Figure S6c) gave a Pb to S molar ratio of about 1:1, consistent with the stoichiometry of a PbS crystal. Our proposed model for the formation of a 3D array of PbS nanoparticles in OU-880 is illustrated in Figure S6d.

Since the formation of the hexagonal 3D assembly of bacteriophage in the resulting silica was governed by charge density matching between the bacteriophage surface and silica species, it was anticipated that fine controlling of the resulting silica structures could be achieved by control of the bacteriophage surface charge properties, which can be fulfilled by displaying differently charged peptides on the side walls. In our experiment, control of the bacteriophage surface charge density was achieved through genetic engineering of the about 3000 copies of pVIII on the side wall of the *M13* bacteriophage. Fusion of a foreign peptide to the N-terminal of pVIII on the bacteriophage was acquired by inserting a single DNA fragment that encoded the foreign peptide sequence into the phage DNA. In this manner, we displayed eight negatively charged glutamate residues (*E8-M13*) or four positively charged arginine residues (*R4-M13*) on the side walls of bacteriophage. Thus, three bacteriophages were prepared with different negative charge densities in the following order: *E8-M13* > *M13* (wild-type) > *R4-M13*. This order was also confirmed by zeta potential measurements. The purified engineered bacteriophage (*E8-M13* and *R4-M13*) and wild-type *M13* were used to prepare silica under conditions similar to those for the preparation of OU-880.

Electron microscopy images exhibited remarkable morphological evolution and obvious change of the bacteriophage assembly pattern in the resulting silica nanofibers (see the Supporting Information for explanation of the mechanism). For example, silica fibers with a length of 2–3 μm, 10–15 μm, and about 1 μm were obtained when *E8-M13*, *M13*, and *R4-M13* bacteriophages were employed as templates, respectively (Figure 3a,c,and e). The TEM micrographs revealed that the surface charge properties of bacteriophages influenced the virus assembly in the presence of APTES, thus controlling the pore structures of the resulting silica nanotubes. Parallel aligned viruses were observed in the *E8-M13* templated silica nanofibers (Figure 3b), whereas wild-type *M13* bacteriophage were assembled into bundle-like structures (Figure 3d). As expected, APTES did not induce aggregation of the bacteriophage *R4-M13*. When *R4-M13* bacteriophages were used as templates, uniform silica nanofibers with a length of 1 μm containing a single virus within each individual silica nanofiber were observed (Figure 3f).

To further understand the virus alignment patterns in the resulting silica structures, bacteriophages (*M13* and *E8-M13*)

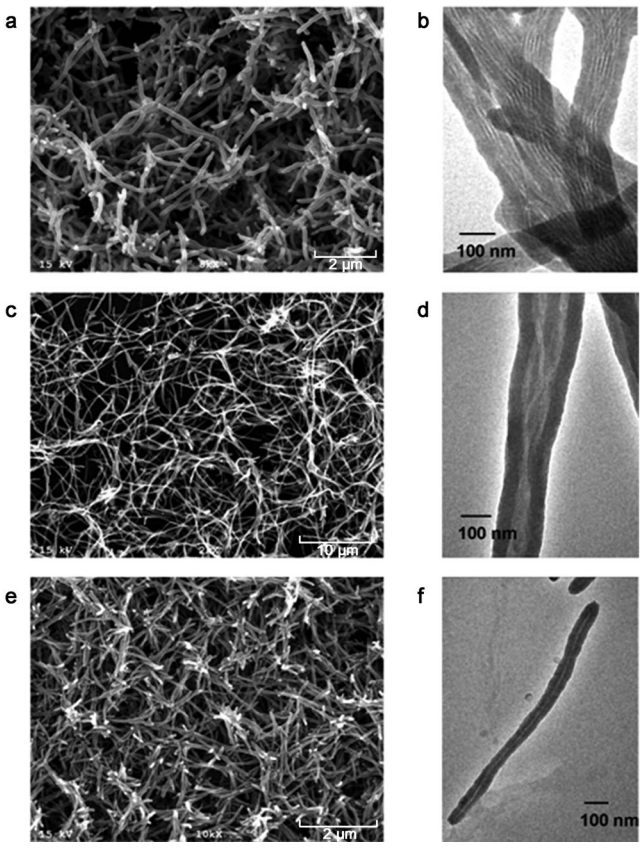

Figure 3. Electron microscopy of silica fibers synthesized by employing *E8-M13* (a, SEM, b, TEM), wild-type *M13* (c, SEM; d, TEM), and *R4-M13* bacteriophages (e, SEM; f, TEM) as templates. *E8-M13* and *R4-M13* are bacteriophages that display anionic and cationic peptides on the side walls, respectively.

were conjugated with Alexa Fluor 488-labeled anti-pIII antibody that recognizes pIII (the tip of phage). The dye-labeled bacteriophages were employed as templates to prepare silica fibers under the same conditions as described above. The fluorescence images of the obtained silica were consistent with TEM images (Figure 3) and confirm the proposed assembly of bacteriophages in silica (Figure S7 in the Supporting Information). For the silica fibers with bundle-aligned viruses (Figure 3 d), the whole fiber is fluorescent as shown in Figure S7 B. In this kind of structure, viruses (*M13* bacteriophage) were supposed to align in a nematic structure, with fluorescent dyes evenly distributed along the fiber. However, for the silica fibers with defined layers (Figure S7 C), there is a smectic alignment of viruses (*E8-M13* bacteriophage) as can be seen from the periodic alignment of the dyes along the fiber, with an interval distance of 800–1000 nm, which is consistent with the length of a single phage (Figure S7 D). However, the silica fibers prepared from the antibody conjugated phages are shorter than the fibers from phages without conjugation, generally in the range of 1 to 2 μm. This may be due to the disturbance of the antibody.

To the best of our knowledge, this is the first successful synthesis of nanostructured mesoporous silica with hexagonally aligned pore structures using biotemplates through a synergistic co-assembly of the bacteriophage and silica precursor species. This particular method can provide new families of mesoporous materials for potential applications in photonic and electronic nanodevices, drug release, and bioreactors. Furthermore, we demonstrated the versatility of the bacteriophage in controlling the nanostructures of silica by controlling the assembly behavior through the surface charge. Thus, great promise is seen in the future for the preparation of inorganic materials with structural diversity.

Experimental Section

The general procedure for synthesizing mesoporous silica: The display of peptides on the side wall of phage was reported in our earlier publication.[24] APTES was added to an aqueous solution of virus (20 mg mL^{-1}, determined using spectrophotometry with an absorption coefficient of 3.84 cm^2 mg^{-1} at 269 nm) at room temperature. The solution was then mixed by vortexing for about 3 min and kept in an ice-water bath for about 10 min. Next, prehydrolyzed TEOS with a final concentration of 0.1 M was added and mixed by vortexing for another 3 min. The resulting mixture was allowed to stand at room temperature for 8 h. Generally, the solution became an opalescent gel after 15 min because of the formation of long silica fibers. Shaking broke the gel to form suspended flocculates which were then taken out by centrifugation and washed with water and ethanol.

Received: November 7, 2011
Published online: May 29, 2012

Keywords: biomineralization · nanomaterials · silica · template synthesis

[1] C. T. Kresge, M. E. Leonowicz, W. J. Roth, J. C. Vartuli, J. S. Beck, *Nature* **1992**, *359*, 710–712.
[2] D. Y. Zhao, J. L. Feng, Q. S. Huo, N. Melosh, G. H. Fredrickson, B. F. Chmelka, G. D. Stucky, *Science* **1998**, *279*, 548–552.
[3] S. Che, A. E. Garcia-Bennett, T. Yokoi, K. Sakamoto, H. Kunieda, O. Terasaki, T. Tatsumi, *Nat. Mater.* **2003**, *2*, 801–805.
[4] a) M. Hartmann, *Chem. Mater.* **2005**, *17*, 4577–4593; b) B. G. Trewyn, I. I. Slowing, S. Giri, H. T. Chen, V. S. Y. Lin, *Acc. Chem. Res.* **2007**, *40*, 846–853; c) J. Y. Ying, C. P. Mehnert, M. S. Wong, *Angew. Chem.* **1999**, *111*, 58–82; *Angew. Chem. Int. Ed.* **1999**, *38*, 56–77.
[5] a) Y. Wan, D. Y. Zhao, *Chem. Rev.* **2007**, *107*, 2821–2860; b) A. Monnier, F. Schuth, Q. Huo, D. Kumar, D. Margolese, R. S. Maxwell, G. D. Stucky, M. Krishnamurty, P. Petroff, A. Firouzi, M. Janicke, B. F. Chmelka, *Science* **1993**, *261*, 1299–1303.
[6] a) F. Wang, D. Li, S. Newton, P. Klebba, C. B. Mao, *Adv. Funct. Mater.* **2008**, *18*, 4007–4013; b) F. Wang, C. B. Mao, *Chem. Commun.* **2009**, 1222–1224; c) Z. Niu, S. Kabisatpathy, J. He, L. A. Lee, J. Rong, L. Yang, G. Sikha, B. N. Popov, T. S. Emrick, T. P. Russell, Q. Wang, *Nano Res.* **2009**, *2*, 474–483.
[7] J. X. Tang, S. Fraden, *Liq. Cryst.* **1995**, *19*, 459–467.
[8] M. Sarikaya, C. Tamerler, A. K. Y. Jen, K. Schulten, F. Baneyx, *Nat. Mater.* **2003**, *2*, 577–585.
[9] a) N. Kroger, R. Deutzmann, M. Sumper, *Science* **1999**, *286*, 1129–1132; b) F. E. Round, R. M. Crawford, D. G. Mann, *The Diatoms: Biology & Morphology of the Genera*, Cambridge University Press, Cambridge, **1990**.
[10] C. E. Flynn, S. W. Lee, B. R. Peelle, A. M. Belcher, *Acta Mater.* **2003**, *51*, 5867–5880.
[11] Z. Dogic, K. R. Purdy, E. Grelet, M. Adams, S. Fraden, *Phys. Rev. E* **2004**, *69*, 051702.

[12] a) Z. Dogic, S. Fraden, *Curr. Opin. Colloid Interface Sci.* **2006**, *11*, 47 – 55; b) Z. Dogic, S. Fraden, *Phys. Rev. Lett.* **1997**, *78*, 2417 – 2420.
[13] L. A. Day, C. J. Marzec, S. A. Reisberg, A. Casadevall, *Annu. Rev. Biophys. Biophys. Chem.* **1988**, *17*, 509 – 539.
[14] R. E. Webster, *Display of Peptides and proteins*, Academic Press, London, **1996**.
[15] a) G. P. Smith, V. A. Petrenko, *Chem. Rev.* **1997**, *97*, 391 – 410; b) C. B. Mao, A. Liu, B. Cao, *Angew. Chem.* **2009**, *121*, 6922 – 6943; *Angew. Chem. Int. Ed.* **2009**, *48*, 6790 – 6810; c) T. He, G. Abbineni, B. Cao, C. B. Mao, *Small*, **2010**, *6*, 2230 – 2235; d) H. Zhu, B. Cao, Z. Zhen, A. Laxmi, D. Li, S. Liu, C. B. Mao, *Biomaterials*, **2011**, *32*, 4744 – 4752.
[16] C. E. Fowler, W. Shenton, G. Stubbs, S. Mann, *Adv. Mater.* **2001**, *13*, 1266 – 1269.
[17] S. Lei, J. Zhang, J. R. Wang, J. B. Huang, *Langmuir* **2010**, *26*, 4288 – 4295.
[18] Y. Qiao, H. F. Chen, Y. Y. Lin, Z. Y. Yang, X. H. Cheng, J. B. Huang, *J. Phys. Chem. C* **2011**, *115*, 7323 – 7330.
[19] a) M. B. Dickerson, K. H. Sandhage, R. R. Naik, *Chem. Rev.* **2008**, *108*, 4935 – 4978; b) M. M. Tomczak, D. D. Glawe, L. F. Drummy, C. G. Lawrence, M. O. Stone, C. C. Perry, D. J. Pochan, T. J. Deming, R. R. Naik, *J. Am. Chem. Soc.* **2005**, *127*, 12577 – 12582.
[20] a) J. N. Cha, G. D. Stucky, D. E. Morse, T. J. Deming, *Nature* **2000**, *403*, 289 – 292; b) R. A. Caruso, M. Antonietti, *Chem. Mater.* **2001**, *13*, 3272 – 3282; c) D. E. Morse, *Trends Biotechnol.* **1999**, *17*, 230 – 232.
[21] a) M. Sumper, N. Kroger, *J. Mater. Chem.* **2004**, *14*, 2059 – 2065; b) M. Sumper, *Science* **2002**, *295*, 2430 – 2433.
[22] Q. S. Huo, D. I. Margolese, U. Ciesla, P. Y. Feng, T. E. Gier, P. Sieger, R. Leon, P. M. Petroff, F. Schuth, G. D. Stucky, *Nature* **1994**, *368*, 317 – 321.
[23] a) Y. J. Han, J. M. Kim, G. D. Stucky, *Chem. Mater.* **2000**, *12*, 2068 – 2069; b) N. R. B. Coleman, N. O'Sullivan, K. M. Ryan, T. A. Crowley, M. A. Morris, T. R. Spalding, D. C. Steytler, J. D. Holmes, *J. Am. Chem. Soc.* **2001**, *123*, 7010 – 7016.
[24] A. Liu, G. Abbineni, C. B. Mao, *Adv. Mater.* **2009**, *21*, 1001 – 1005.

